Scanning-tunneling-microscope observation of the homoepitaxial diamond (001) 2×1 reconstruction observed under atmospheric pressure

Hiroshi Kawarada, Hidehiro Sasaki, and Atsuhiro Sato
School of Science and Engineering, Waseda University, Ohkubo 3-4-1, Shinjuku-ku, Tokyo 169, Japan
(Received 9 March 1995; revised manuscript received 13 June 1995)

The 2×1/1×2 surface reconstruction of a homoepitaxial diamond (001) surface has been examined using a scanning tunneling microscope at an atomic scale and reflection electron microscopy at a macroscopic scale. The monohydride dimer, which is a unit of the surface reconstruction, has a symmetric structure. These monohydride structures contribute to the surface *p*-type conduction in undoped films. The surface is composed of elongated dimer rows. Antiphase boundaries have been observed, which is indicative of low-temperature epitaxy where surface migration is limited. Macroscopic surface flatness has been improved during the growth stage in the presence of oxygen and boron which enhance migration.

I. INTRODUCTION

The 2×1/1×2 surface reconstruction of diamond (001) surfaces was first observed by Lurie and Wilson[1] using low-energy electron diffraction. The surface was reported to be clean and the participation of hydrogen in the reconstruction was not mentioned. After chemical vapor deposition (CVD) of diamond has been established, the reconstruction is reproducibly observed on hydrogenated surfaces[2] or as-grown surfaces even after being exposed in air.[3] The first atomic-scale scanning-tunneling-microscope (STM) image of the diamond (001)-2×1 surface taken in air revealed that the reconstruction is due to dimer atoms.[4] The 2×1 reconstruction formed after the CVD process is explained in terms of the monohydride dimer, because C-H vibration is observed by several methods[5,6] after the process. The dimer is the smallest unit in the surface reconstruction. A schematic model of the (001)-2×1 structure composed of balls an sticks is shown in Fig. 1. The topmost layer forms monohydride dimers and the dimers form a row. Hydrogen termination is thought to be effective in stabilizing the diamond phase during the vapor growth process.

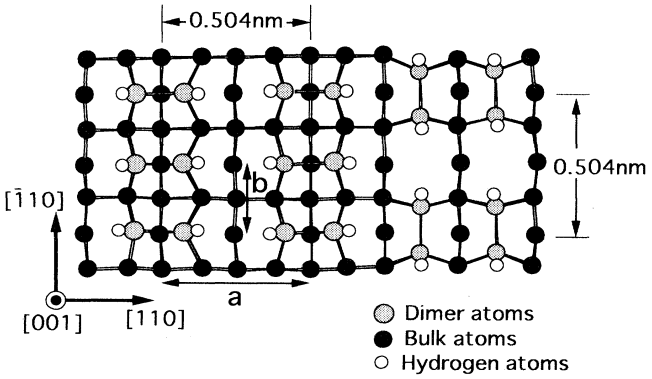

FIG. 1. Ball and stick model of diamond (001) 2×1:H reconstructed surface. $a \times b$ shows a unit area.

While the atomic-scale STM observations of Si (Ref. 7) or Ge (Ref. 8) surfaces have been carried out in detail to discuss the homoepitaxial growth processes, those of diamond surfaces have been carried out only in limited cases.[9–15] One of the reasons is that diamond films obtained on nondiamond substrates are generally polycrystalline. However, even in polycrystalline films, dimer rows on {001} facets and hexagonal structures on {111} surfaces have been frequently observed.[9,11] This indicates that the surfaces are composed of these low-index planes at an atomic scale and that the growth occurs mainly at these two planes. Recently we presented the atomic STM images of the (111) surface of homoepitaxial layers where adsorbates are clearly observed at an atomic scale,[13] which are assumed to be growth precursors. A comparative study of the (001) surfaces with the (111) surfaces is needed to consider the growth kinetics, using homoepitaxial films from which more general information can be obtained.

Another topic concerning the diamond surfaces is the hydrogen-termination effect on electronic properties. Hydrogen termination is expected to eliminate the surface dangling bonds and to reduce the number of defect sites that are detrimental for semiconducting device applications. We recently reported that excellent Schottky diodes[15,16] and metal semiconductor field-effect transistors[17] can be obtained using the hydrogen-terminated (001)-2×1 surfaces, for the first time. In both cases, the *p*-type semiconducting surfaces of undoped homoepitaxial films are used for hole conduction. The mechanism of surface conduction[18] is still puzzling, but it is certain that the conduction is related to hydrogen termination, for example, surface band bending due to hydrogen termination at the surface is proposed.[19] Tunneling currents can be obtained through the *p*-type surface semiconductive layer. Thus, the surface characterization of (001)-2×1 surfaces using STM is important not only in the diamond growth mechanism, but also for electronic applications.

In this study, atomic-scale STM study of (001) surfaces has been carried out in combination with macroscopic studies using reflection electron microscopy (REM). The

0163-1829/95/52(15)/11351(8)/$06.00

flatness of (001) surfaces, microscopic surface growth mode, adsorbates, and surface electronic structures have been discussed for the smoothest diamond (001) surfaces formed by homoepitaxial growth.

II. EXPERIMENT

Homoepitaxial diamond films have been grown by microwave plasma CVD. The reaction gas was CO(5%) or CH_4(5%) diluted with H_2. The total gas flow rate was normally 0.2 l/min and the pressure was 35 Torr. The substrates were high-pressure synthetic diamond (001) ($1.5\times2.0\times0.3$ mm in size). The substrate temperatures were kept at around 800–900 °C during deposition. Boron doping was carried out in some samples by B_2H_6 during deposition. Boron/carbon (B/C) ratios in the gas phase were 1000–2000 ppm and the dosage of boron was about $(1-2)\times10^{18}$ cm^{-3}. The deposition time was normally 3 h and the resultant film thickness was about 1 μm.

The depositions are completed with pure hydrogen plasma treatment at 35 Torr for 1 min to remove nondiamond carbon layers that are formed by residual carbon gas during the temperature decreasing process. The obtained surfaces are hereafter called "as-grown surfaces" *p*-type surface conduction is observed on the surfaces of undoped films. The popular surface oxidation treatment, such as CrO_3 treatment, was not carried out in our case in order not to destroy hydrogen termination. Tunneling currents for STM measurements are supplied from the surface semiconducting layer, especially in the undoped samples.

The surfaces of homoepitaxial CVD diamond films have been characterized using an atomic-scale STM (Seiko SAM 3000). Two typical scanning modes were used. One is a constant-current scan where the *z* movement of the tip is recorded and the other is a constant-height scan where the tunneling current is monitored. Hereafter, we call images obtained in the modes "topographic image" and "current image," respectively. Macroscopic surfaces were observed using REM (JEM 100 CX) operated at 100 kV.

III. RESULTS AND DISCUSSION

A. Macroscopic surface flatness

The surface structures of (001) diamond films have been characterized from reflection high-energy electron diffraction (RHEED) patterns. The RHEED patterns from [110] of undoped homoepitaxial films formed by CH_4 (5%)/H_2 shows that the streaky (0,1/2) spots due to a 2×1 structure have been observed in the zeroth-order Laue zone. The same result has been obtained in the observation from [$1\bar{1}0$]. However, the spots expected in the half-order Laue zone are not present. The surface has been reconstructed to $2\times1/1\times2$ structure, but is not smooth enough to produce the elongated reciprocal rods observed as the half-order Laue spots.

The half-order Laue pattern is observed on the films formed from CO(5%)/H_2. Among them, boron-doped films flow distinct half-order Laue patterns. Figures 2(a) and 2(b) show the RHEED patterns of boron-doped homoepitaxial films on (001) diamond formed from CO(5%)/H_2. The B/C ratios are 1000 and 2000 ppm in Figs. 2(a) and 2(b), respectively. Boron concentrations in the films are measured to be $(1-2)\times10^{18}$ cm^{-3}. The streaky spots in the half-order Laue pattern in Fig. 2(b) indicate that the 1×2 domains are narrow in the direction of electron incidence, [110] direction in this case, and elongated in the [$1\bar{1}0$] direction.

The surface morphology has been investigated from REM images shown in Fig. 3. The surface of the substrates before diamond deposition is shown in Fig. 3(a). The stripes appearing in the surface are scratches formed in the diamond polishing process. The roughness of the surface is about 10 nm in this case. The 2×1 reconstruction is observed after 15 min hydrogen plasma treatment.

The morphology of the surface has been changed by homoepitaxial growth. Figure 3(b) shows the REM image of a layer grown homoepitaxially using CH_4(5%)/H_2. Although the amount of surface stripes decreases, a wavy structure remains on the surface. In the film formed from CO(5%)/H_2, the surface flatness is improved and the contrast of the stripes is weakened. In boron-doped

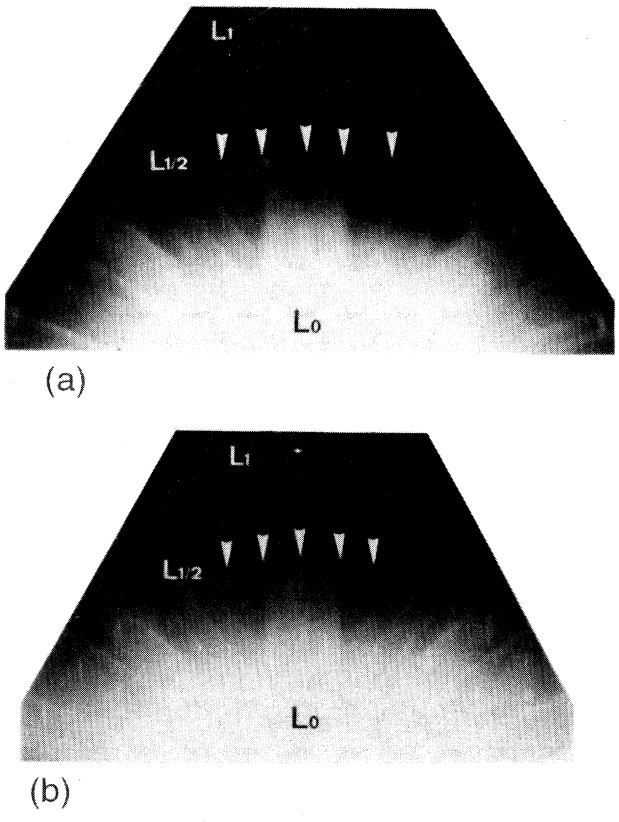

FIG. 2. RHEED patterns of the boron-doped and as-grown homoepitaxial films formed by CO(5%)/H_2. The B/C ratio in the ambient: (a) 1000 ppm and (b) 2000 ppm. The spots at the half-order Laue zone are observed.

films formed from $CO(5\%)/H_2$ with a B/C ratio of 1000–2000 ppm, the surface is smooth and the wavy structure has been minimized in the present experiment. Usually these homoepitaxial layers are observed to be very smooth in high-resolution scanning electron microscopy. The REM is very sensitive to the small roughness of the surfaces.

The improvement of the crystallinity upon doping of boron during growth has been reported in some experiments.[20] Enhanced surface diffusion of carbon atoms has been suggested on the basis of a theoretical calculation

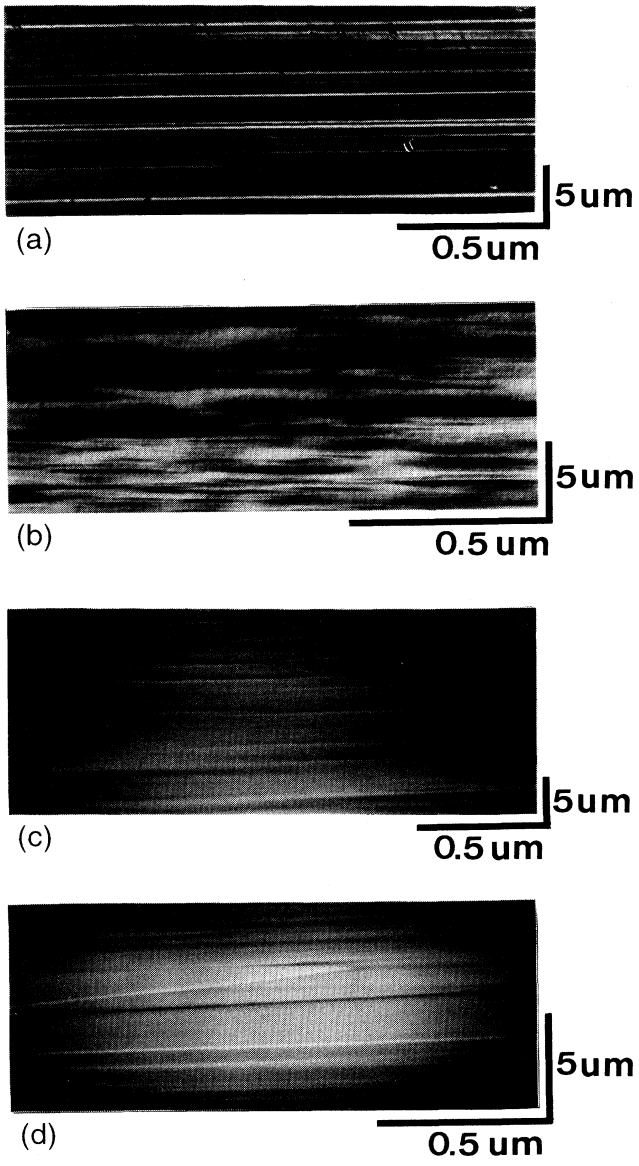

FIG. 3. Reflection electron microscope images on the as-grown diamond (001) surfaces: (a) high-pressure synthetic diamond substrate immersed in H_2 plasma for 15 min; (b) undoped homoepitaxial diamond films formed from $CH_4(5\%)/H_2$; (c) undoped homoepitaxial diamond formed from $CO(5\%)/H_2$; (d) boron-doped homoepitaxial diamond formed from $CO(5\%)/H_2$. The B/C ratio is 2000 ppm.

basis that indicates the lowering of migration energy in *p*-type or *n*-type diamonds.[21] The results shown in Figs. 2 and 3 can be explained by the migration enhancement.

B. Atomic STM images and surface *p*-type conduction

The STM images of undoped and as-grown homoepitaxial diamond films are shown in Figs. 4(a), 4(b), and 4(c). In the 25×25-nm scanned current image [Fig. 4(a)], the dimer rows of the (001)-2×1 surface are elongated toward the [110] and [1$\bar{1}$0] directions, forming double domains. This kind of image is reproducibly observed from as-grown (001) surfaces of homoepitaxial diamonds if tip conditions are optimized. The upper left part of Fig. 4(a) is higher than the lower right part. In Fig. 4(b) (10×10-nm scanned topographic image), the total length of S_A steps is observed to be longer than that of S_B steps (marked *a*). The aspect ratio of S_A to S_B is as high as 3 on average. The two short chains marked *b* suggest that nucleation of dimers on terraces may occur at a rate comparable to that of addition of dimers to the ends of rows. This feature resembles that of the lower-temperature homoepitaxy of Si.[22] It appears that growth occurs preferentially at the S_B steps, but surface migration is limited. The anisotropic probability of sticking plays a dominant role in the case of the diamond (001) surface. The average terrace size of this sample is less than 10 nm. The adsorbates, which are frequently observed on the (111) surfaces[13] formed under the same growth conditions as those on the (001) in the present work, are not observed in Fig. 4(b).

Figure 4(c) shows a current image of the 2.5×2.5-nm scanned area where individual dimers of the 2×1 structure are resolved and observed to be oval. Atoms of a dimer are not resolved in this image. The distance between two dimer rows (marked *a*) is 0.5 nm, and that between two dimers (marked *b*) is 0.25 nm. These values correspond to the lengths of *a* and *b* in Fig. 1. A missing dimer defect as observed on Si(001)-2×1 surface[23] has been imaged on the right-hand side of Fig. 4(c).

Figure 5(a) shows typical current-voltage (*I-V*) characteristics for undoped and as-grown diamond (001) obtained at different tip-sample separations. Every curve has been reproducibly observed to be asymmetric. While the current increases rapidly at negative sample bias, it remains low at positive sample bias. This asymmetrical nature of the *I-V* curves indicates a large-band-gap material having *p*-type conduction. At a small tip-sample separation [curves *a* and *b* in Fig. 5(a)] where atomic images such as Fig. 4 are obtained, the *I-V* curves exhibit, in addition to the asymmetric nature, a distinct current increase above the Fermi level (0-V bias). This type of *I-V* curve (curve *a* or *b*) shown in Fig. 5(a) is not localized at a particular place, but is reproducibly observed for the general dimer rows of the (001)-2×1 surfaces. The steep slope at 0–1.0-V bias shows a surface-state-related feature.

Figure 5(b) shows a $(dI/dV)/(I/V)$-V curve corresponding to *I-V* curve *a* in Fig. 5(a). The shaded area appears to be part of a valence-band edge, because the minimum of $(dI/dV)/(I/V)$ at 0-V bias is caused not

only by the decrease of the slope (dI/dV) with the approach to 0 V from the negative side but also by $V=0$. However, the peak above 0 V in Fig. 5(b) is due to the rapid rise of current. Thus, the shaded area can be considered as a state other than the band edge. This type of state is reproducibly observed using STM at dimerized structures of (001) surfaces and monohydride (111) surfaces[13] formed under the same growth condition.

The spectrum in Figs. 5(b) appears to be similar to that of the ultraviolet photoelectron spectroscopy (UPS) spectrum of the diamond (001) 2×1:H surface, where a strong and broad surface-state feature from 0 to 1.5 eV above the valence-band maximum (VBM) has been observed.[2] However, the states observed in the UPS are filled states while the shaded area in Fig. 5(b) exhibits empty states. Since empty surface states cannot be observed by the UPS, the origin of the surface states might be different from our result. Recently, the surface states measured by UPS has been interpreted in terms of surface hydrogen and carbon atoms of (001)-2×1 using tight-binding calculation.[24] On the other hand, this kind of state cannot be found in the energy gap of the monohydride dimer structures in two *ab initio* theoretical calculations.[25,26] In both results, surface dangling bonds are indicated to be responsible for the surface states. However, dangling bonds are not stable in air and can

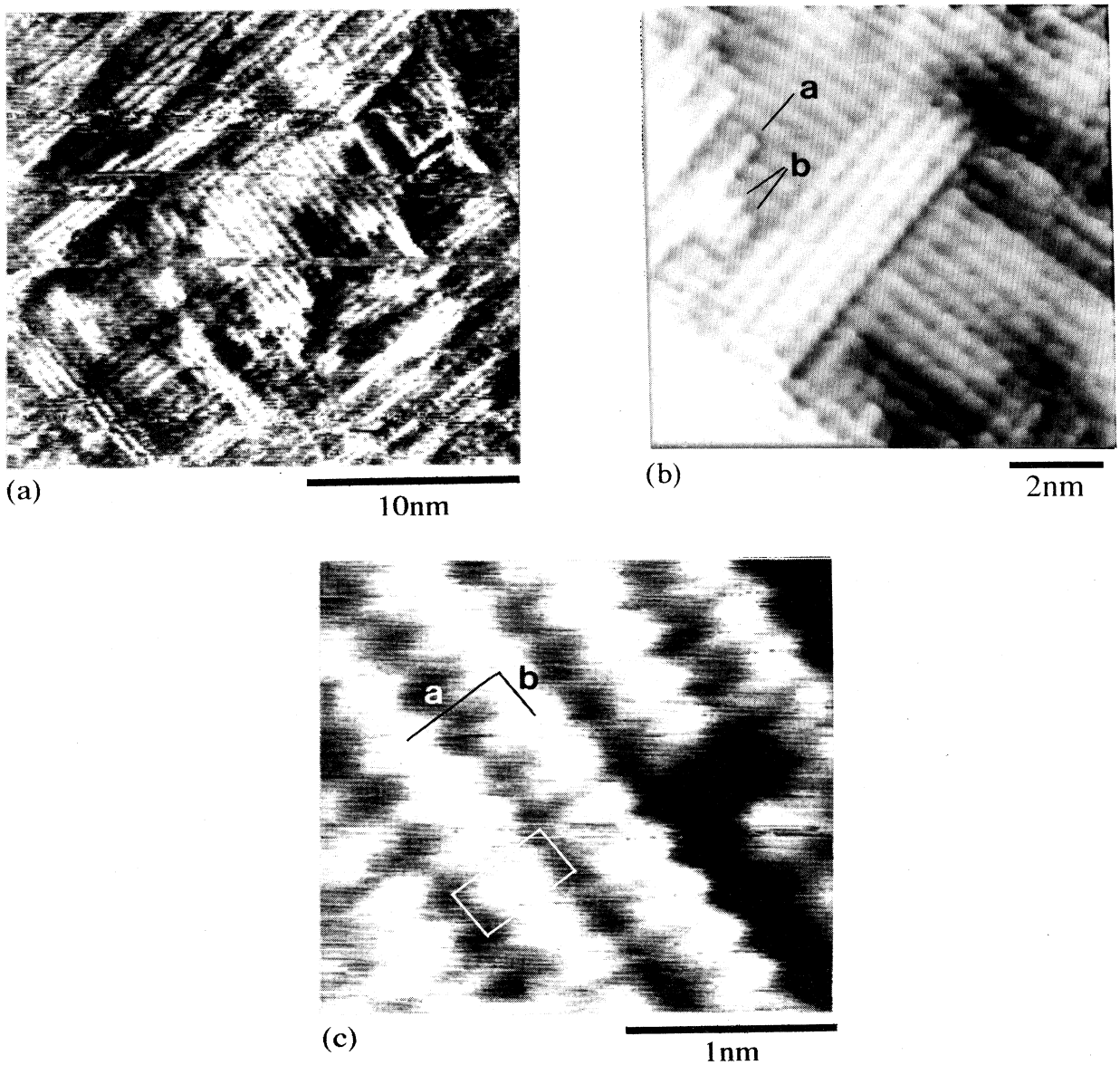

FIG. 4. STM images of undoped and as-grown CVD diamond (001) surfaces formed from CO(5%)/H_2. (a) Current image of 25×25-nm scanned area. The sample bias and tunneling current were −0.05 V and 1 nA. (b) Topographic image of 10×10-nm scanned area. The sample bias and tunneling current were −0.1 V and 3 nA. (c) Current image of 2.5×2.5-nm scanned area. High-magnification image of dimer rows. The length a is 0.5 nm and b is 0.25 nm. The sample bias and tunnel current were −0.05 V and 1 nA.

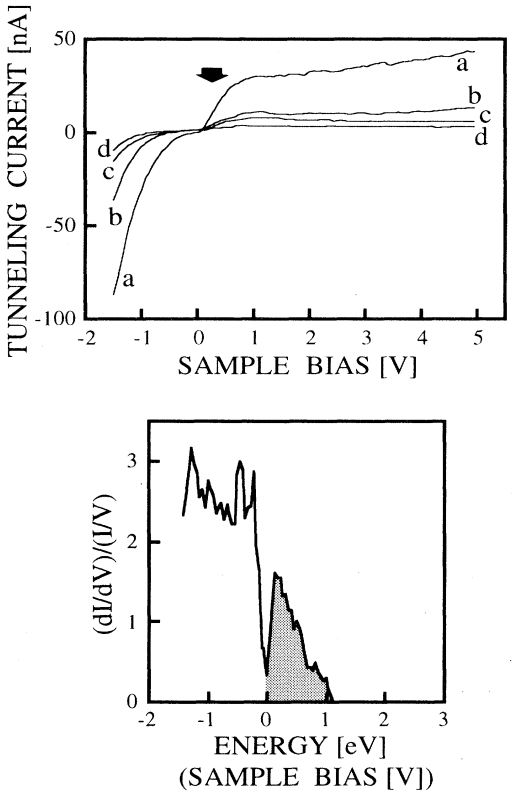

FIG. 5. (a) Current-voltage characteristics of undoped diamond (001) 2×1:H surfaces at different tip-sample separations. The separation increases from curve *a* to curve *d*. In curves *a*, *b*, *c*, and *d*, 1-nA tunneling current is obtained at sample biases of −0.2, −0.4, −0.6, and −0.8 V, respectively. (b) $(dI/dV)/(I/V)$-voltage characteristic of curve *a*. The hatched area reflects the surface-state-related slopes at 0–1.0-V bias in (a).

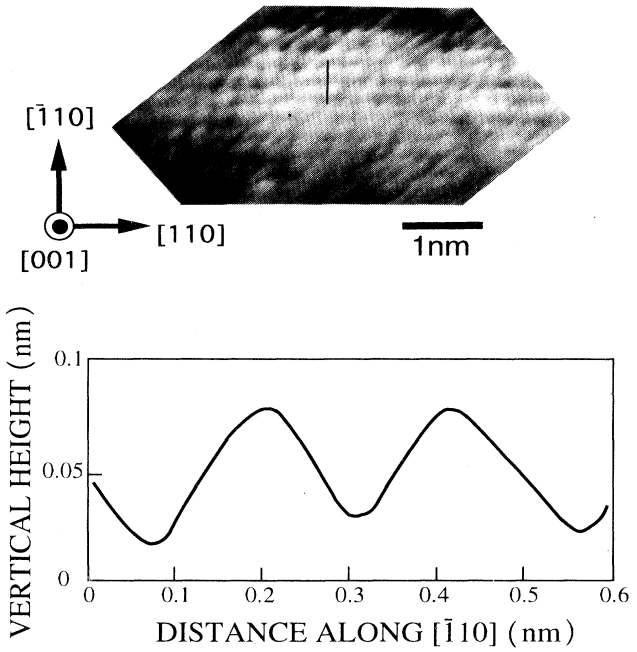

FIG. 6. (a) STM topographic image of undoped and as-grown diamond (001) surfaces formed from CO(5%)/H_2. The substrate bias and tunneling current were 0.5 V and 1 nA. (b) STM corrugation profile of the line marked along the [1$\bar{1}$0] direction.

not be observed in the present STM measurement.

The atomic image taken at the sample bias of 0–1.0 eV represents the position of this special state. Figure 6 shows an atomic topographic image taken at the sample bias of 0.5 V. The atomic image does not show dimer rows as in Fig. 4(c). The distance between the bright spots is 0.23 nm on the average and is comparable to the separation of hydrogen atoms of a monohydride dimer. The distance has been calculated by empirical or semiempirical methods[27,30] and *ab initio* methods.[25,31]

In the simple tight-binding models using only *s* and *p* orbitals,[32] the antibonding state of C-H bonding is located at 4.6 eV above the VBM, while the H 1*s* level is at 0.2 eV above the VBM. The dangling-bond state is almost the same level as that of H 1*s*. The energy level of the C-H antibonding state is far from the empty states just above 0 V. On the other hand, the position of the H 1*s* orbital is the closest to the states energetically and to the tip spatially. The observed dots in the STM image obtained at 0.5-V sample bias can be interpreted as the orbitals belonging to surface hydrogen atoms.

Hydrogen-induced surface states of acceptor type have been observed in GaAs.[33] This kind of hydrogen-induced surface acceptors may be related to the *p*-type conduction of undoped diamond films. If acceptor-type surface states are present around the VBM, the energy levels of the surface acceptors are below the Fermi level and charge negatively [Fig. 7(a)]. To satisfy the surface

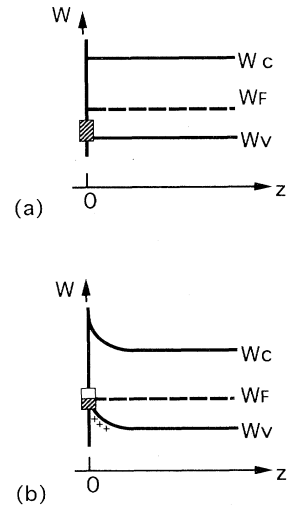

FIG. 7. Schematic of band diagram of undoped diamond surface where acceptor-type surface states are present. The bulk Fermi level is located at about 2.0 eV above the valence band top in this figure. (a) Before band bending. (b) After band bending to satisfy charge neutrality.

charge neutrality, upward band bending is needed [Fig. 7(b)]. This bending moves the surface acceptor levels closer to the Fermi level to become partially neutral, i.e., empty. This neutralized acceptor level shown as a blank in the schematic surface states in Fig. 7(b) can be observed as empty states just above 0 V in Fig. 5(b). Moreover, band bending causes an accumulation of holes, because other space charges are negligibly present in the undoped diamond. The accumulated holes compensate the net charge in the surface acceptors so that the condition of surface charge neutrality is satisfied. We speculate that the empty surface states observed in Fig. 5 are related to the upward band bending, which can explain the *p*-type conduction in undoped diamonds having the monohydride surface. The hole conductivity of the undoped diamond does not depend on the temperature in the range of 150–450 K,[34] indicating the presence of acceptor levels around the VBM.

Three typical STM images of boron-doped and as-grown diamond films are shown in Figs. 8(a), 8(b), and 8(c). These three frame sizes correspond to those of Figs. 4(a), 4(b), 4(c), respectively. Figure 8(a) is a current image of the 25×25-nm scanned area. The surface forms a downward slope from left to right in the image. The surface roughness level is almost the same as that of Fig. 4(a). The macroscopic surface flatness has been improved by the same amount of boron doping, but microscopic morphology is not very different from that of undoped samples. Figure 8(b) is a topographic image of the 10×10-nm scanned area. An isolated dimer row needle-like in appearance is observed (marked *a*). In the middle of the upper half of this image (marked *b*), a uniform-

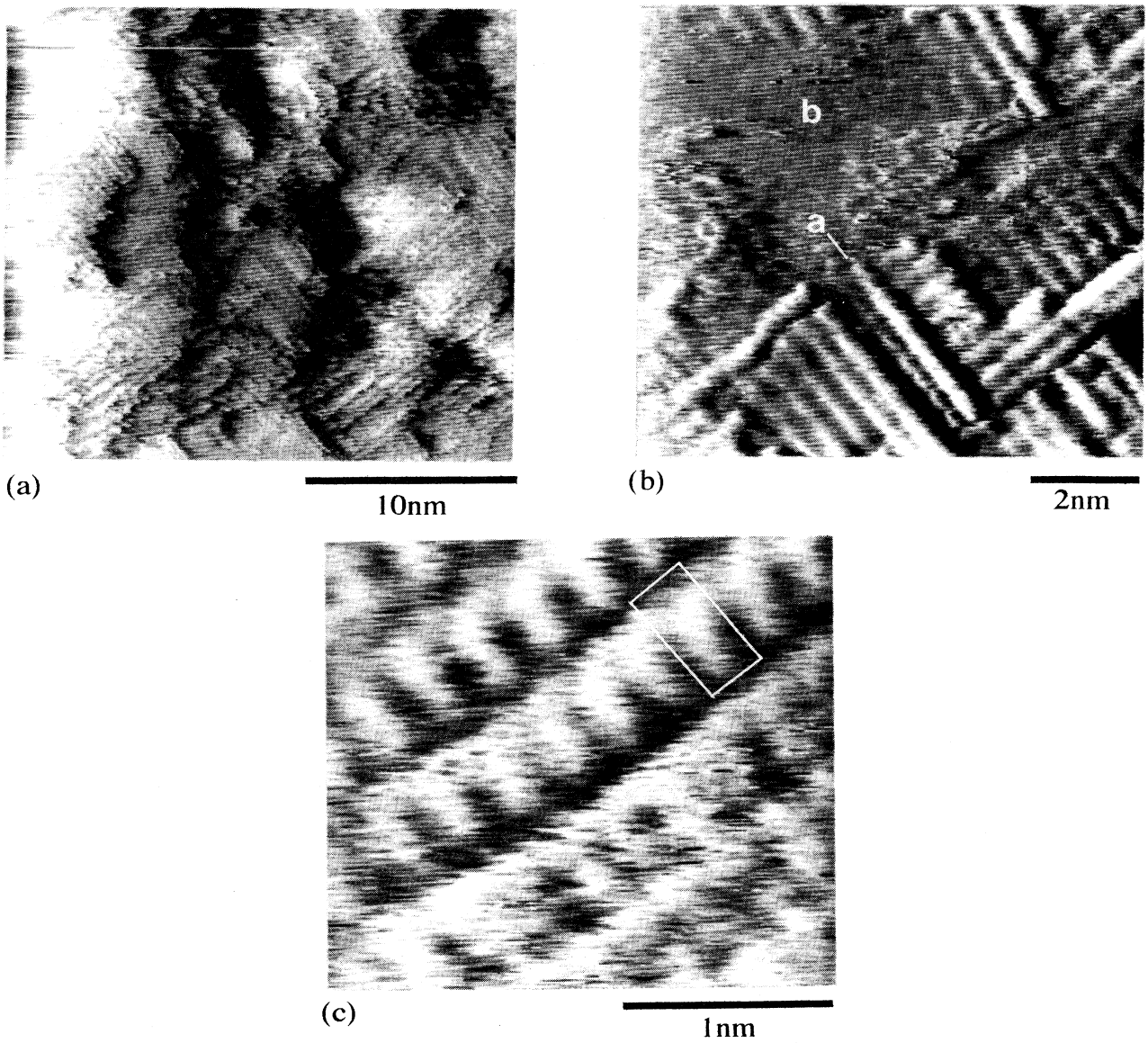

FIG. 8. STM image of boron-doped and as-grown diamond (001) surfaces (B/C 2000 ppm). (a) 25×25-nm scanned area. (b) 10×10-nm scanned area. (c) 2.5×2.5-nm scanned area. All the images were current images obtained at the sample bias of −0.1 V and the tunneling current of 1 nA.

contrast region where dimerization has not been completed is also observed. Figure 8(c) shows well-resolved dimer rows, and the unit rectangle in the image corresponds to one dimer. The STM images of the boron-doped films show no substantial difference from the undoped films in local areas. However, the *I-V* curves of the boron-doped films are different from those of the undoped films at positive sample bias where the tunneling currents have already increased and the large-band-gap nature has disappeared. On the other hand, the structures near 0 V (Fermi level) are the same as those of the undoped film. The same types of surface states are also present.

C. Surface migration and stable structure

Two rotationally equivalent 2×1 domains can be formed on each terrace of the (001) surface, differing only by a translation of 0.25 nm along the [110] direction, because the epitaxial islands nucleate randomly with 50% probability of forming each of the two possible 2×1 domains. Figure 9 shows a discontinuous boundary where the two domains meet. The line drawn on the dimer rows in region *b* is elongated to the trough between the dimer rows in region *a*. The phase of dimer rows shifts by half a period from the others at the boundary. This is the antiphase boundary.

In the case of Si, this type of antiphase boundary is produced at a relatively low substrate temperature.[22] The temperature is not so high that both domains on a terrace cannot coalesce or rearrange to form a single domain. The observation of antiphase boundaries in diamond provides evidence of low-temperature epitaxy where surface diffusion is limited; i.e., long-range correlation of the atomic motion is small.

The substrate temperature (T_s) dependences of homoepitaxial growth modes in group-IV and -III-V semiconductors are classified on the basis of the melting point (T_m) of each material.[35] At $T_S < \frac{1}{4}T_m$, surface diffusion occurs negligibly, and grown films are amorphous or microcrystalline. At $\frac{1}{4}T_m < T_s < \frac{1}{2}T_m$, two-dimensional nucleation on terraces and growth at these ledges are dominant due to the limitation of surface diffusion. The step flow growth mode due to the sufficient surface diffusion appears at $T_s > \frac{1}{2}T_m$. From this criterion, the homoepitaxy of diamond at 800–900 °C can be classified as low-temperature epitaxy if T_m of diamond is assumed to be 4000 K, which is a reasonable value. The surface diffusion length, if present, is very short. A crystal grows by accommodating the adsorbates present within a few migration steps. A large supply of growth species arriving from the ambient is needed, and the anisotropic probability of sticking at step edges might play a dominant role in the case of the (001) surface.

In some areas, a structure that cannot be explained by the dimer rows is present. In Fig. 10, some rows having 0.25-nm spacing were observed to run from the lower left to the upper right, in addition to normal dimer rows. The distance 0.25 nm is half the dimer row spacing. One of the possible structures is a linear arrangement of dihydrides. Another is a mixture of dihydrides and monohydride dimers. Orbitals belonging to hydrogen atoms form line-shaped protrusions.

From our *ab initio* molecular-orbital calculation of carbon dimer models,[31] the total energy of the symmetric monohydride dimer is the lowest, but that of the dihydride is close to that of the monohydride. Yang, Drabold, and Adams[25] have reported that the mixed structure composed of a monohydride dimer and dihydride

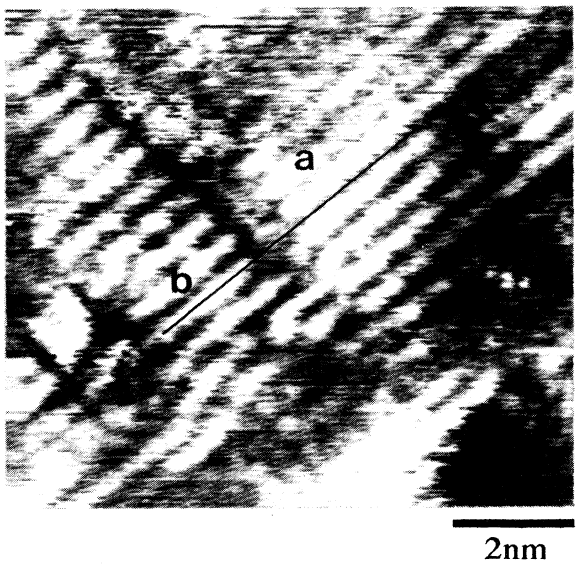

FIG. 9. STM current image of antiphase boundaries on undoped and as-grown diamond film formed from CO(5%)/H_2. The sample bias and tunneling current were −0.05 V and 1 nA.

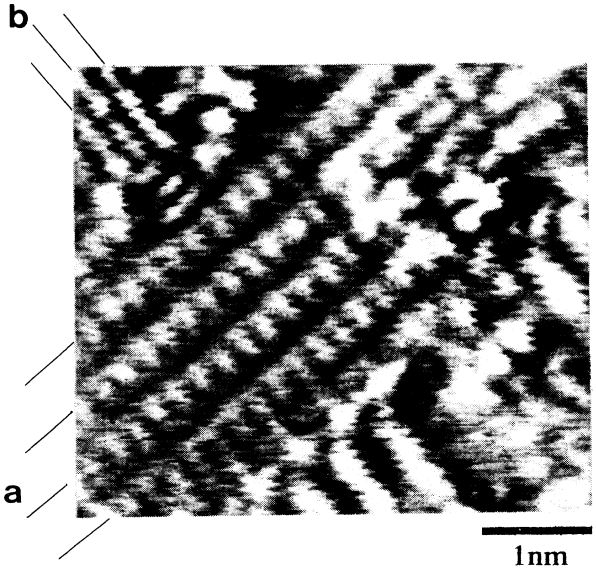

FIG. 10. STM current image of undoped and as-grown diamond formed from CO(5%)/H_2. Dimer rows (*a*) are surrounded by unidentified structure. The spacing of structure *b* is 0.25 nm. Sample bias and tunnel current were −0.05 V and 1 nA.

carbon, i.e., the 3×1:1.33H structure, is more stable than the monohydride dimer (2×1:H structure). At lower substrate temperatures, the probability of the coexistence of dihydrides with monohydrides becomes higher. In some cases, CVD diamonds can grow at a far lower temperature than 800–900 °C (present case). At such a low-temperature epitaxial growth surface, the structure might be very different from $2\times1/1\times2$, because dihydrides are present, and the surface migration is limited to the order of one atomic site.

IV. CONCLUSIONS

We have carried out atomic-resolution STM observation on as-grown homoepitaxial diamond (001) surfaces and the macroscopic surface flatness has been characterized by REM. The following conclusions were derived from the present work. (1) Macroscopic surface flatness can be improved through the choice of the reactant gas and dopant. CO is effective in maintaining surface flatness during epitaxial growth, and boron doping might enhance surface migration. (2) The tunneling current observed from undoped CVD diamond film is due to the p-type surface semiconducting layer. The origin of p-type conduction is related with the surface-state-related feature appearing in the STS spectra. The states are uniformly distributed on the surface and are assumed to be related to C-H bonds. (3) The $2\times1/1\times2$ structure on (001) diamond is composed of dimer rows. The aspect ratio of S_A steps to S_B steps is greater than 3. The observation of antiphase boundaries indicates that the present diamond growth at 800–900 °C can be classified as low-temperature epitaxy. The anisotropic probability of sticking plays a dominant role in the case of the (001) surface. (4) Symmetric monohydride dimers are dominant on the surface grown at 800–900 °C, but there coexist unidentified local structures, some of which are explained by the participation of dihydrides.

ACKNOWLEDGMENTS

The authors are grateful to Mr. T. Yamashita of Tokyo Gas Co., Ltd. and N. Fujimori of Sumitomo Electric Industries, Ltd. for their collaboration. They also thank members of the technical staff, especially M. Suzuki, or Kagami Material Laboratory of Waseda University for their assistance.

[1]P. G. Lurie and J. M. Wilson, Surf. Sci. **65**, 453 (1977).
[2]A. V. Hamza, G. D. Kubiak, and R. H. Stulen, Surf. Sci. **237**, 35 (1990).
[3]H. Shiomi, K. Tanabe, Y. Nishibayashi, and N. Fujimori, Jpn. J. Appl. Phys. **29**, 34 (1990).
[4]T. Tsuno, T. Imai, Y. Nishibayashi, K. Hamada, and N. Fujimori, Jpn. J. Appl. Phys. **30**, 1063 (1991).
[5]T. Ando, M. Ishii, M. Kamo, and Y. Sato, J. Chem. Soc. Farday Trans. **89**, 1783 (1993).
[6]T. Aizawa, T. Ando, M. Kamo, and Y. Sato, Phys. Rev. B **48**, 18 348 (1993).
[7]R. J. Hammers, R. M. Tromp, and J. E. Demuth, Phys. Rev. B **34**, 5343 (1986).
[8]J. A. Kubby, J. E. Griffith, R. S. Becker, and J. S. Vickers, Phys. Rev. B **36**, 6079 (1987).
[9]H. G. Maguire, M. Kamo, H. P. Lang, E. Meyer, K. Weissendanger, and H. J. Guntherodt, Diam. Relat. Mater. **1**, 634 (1992).
[10]H.-G. Busmann, W. Zimmermann-Edling, H. Sprang, H. J. Güntherodt, and I. V. Hertel, Diam. Relat. Mater. **1**, 979 (1992).
[11]W. Zimmermann-Edling, H.-G. Busmann, H. Sprang, and I. B. Hertel, Ultramicroscopy **42-44**, 1366 (1992).
[12]H.-G. Busmann, S. Lauer, I. V. Hertel, W. Zimmermann-Edling, H. J. Güntherodt, Th. Frauenheim, P. Blaudeck, and D. Porezag, Surf. Sci. **295**, 340 (1993).
[13]H. Sasaki and H. Kawarada, Jpn. J. Appl. Phys. **32**, L1771 (1993).
[14]T. Tsuno, T. Tomikawa, S. Shikata, T. Imai, and N. Fujimori, Appl. Phys. Lett. **64**, 572 (1994).
[15]H. Kawarada, M. Aoki, H. Sasaki, and K. Tsugawa, Diam. Relat. Mater. **3**, 961 (1994).
[16]M. Aoki and H. Kawarada, Jpn. J. Appl. Phys. **33**, L708 (1994).
[17]H. Kawrarada, M. Aoki, and M. Ito, Appl. Phys. Lett. **65**, 1563 (1994).
[18]M. I. Landstrass and K. V. Ravi, Appl. Phys. Lett. **55**, 1391 (1989).
[19]T. Sugino, Y. Sakamoto, A. Furukawa, and J. Shirafuji, in *Diamond, SiC and Nitride Wide Bandgap Semiconductors,* edited by C. H. Carter, Jr., G. Gildenblat, S. Nakamura, and R. J. Nemanich, MRS Symposia Proceedings No. 339 (Materials Research Society Pittsburgh, 1994), p. 45.
[20]K. Nishimura, K. Das, and J. T. Glass, J. Appl. Phys. **69**, 3142 (1991).
[21]M. Hata, M. Tsuda, and S. Oikawa, Surf. Sci. **79/80**, 255 (1994).
[22]R. J. Hammers, U. K. Kohler, and J. E. Demuth, J. Vac. Sci. Technol. A **8**, 195 (1990).
[23]R. J. Hammers, Ph. Avouris, and F. Bozso, Phys. Rev. Lett. **59**, 2071 (1987).
[24]V. I. Gavrilenko, Phys. Rev. B **47**, 9556 (1993).
[25]S. H. Yang, D. A. Drabold, and J. B. Adams, Phys. Rev. B **48**, 5261 (1993).
[26]Th. Fraenheim, U. Stephan, P. Blaudeck, D. Porezag, H.-G. Busmann, W. Zimmermann-Edling, and S. Lauer, Phys. Rev. B **48**, 18 198 (1993).
[27]W. S. Verwoerd, Surf. Sci. **108**, 153 (1981).
[28]S. P. Mehandru and A. B. Anderson, Surf. Sci. **248**, 369 (1991).
[29]X. M. Zheng and P. V. Smith, Surf. Sci. **256**, 1 (1991).
[30]Y. L. Yang and M. P. D'Evelyn, J. Vac. Sci. Technol. **10**, 978 (1992).
[31]K. Tsugawa and H. Kawarada, *Transactions of the Materials Research Society of Japan* (Elsevier, Tokyo, 1994), Vol. 14B, p. 1489.
[32]W. Mönch, *Semiconductor Surfaces and Interfaces* (Springer-Verlag, Berlin, 1993), p. 44.
[33]T. U. Kampen, L. Kenders, K. Smith, M. Rückschloss, and W. Mönch, Surf. Sci. **242**, 314 (1991).
[34]K. Hayashi, H. Miyoshi, S. Hara, and H. Okushi, *Extended Abstracts of the 42nd Spring Metting* (Japan Society of Applied Physics, Tokyo, 1995), p. 424.
[35]A. Ishizaka, Jpn. J. Appl. Phys. **27**, 883 (1988).

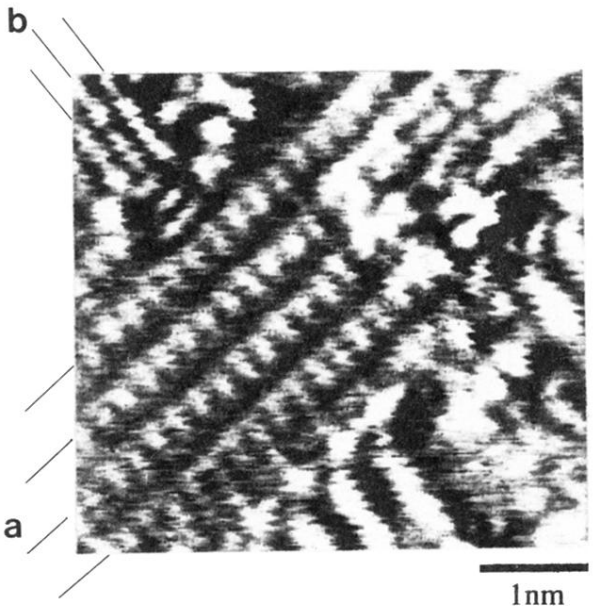

FIG. 10. STM current image of undoped and as-grown diamond formed from CO(5%)/H_2. Dimer rows (*a*) are surrounded by unidentified structure. The spacing of structure *b* is 0.25 nm. Sample bias and tunnel current were −0.05 V and 1 nA.

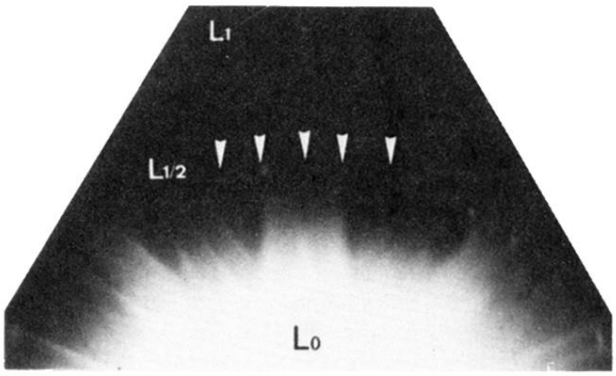

(a)

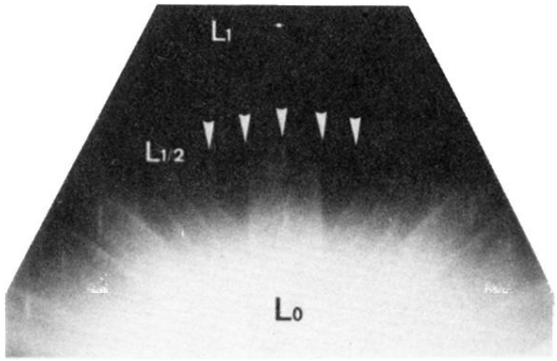

(b)

FIG. 2. RHEED patterns of the boron-doped and as-grown homoepitaxial films formed by CO(5%)/H_2. The B/C ratio in the ambient: (a) 1000 ppm and (b) 2000 ppm. The spots at the half-order Laue zone are observed.

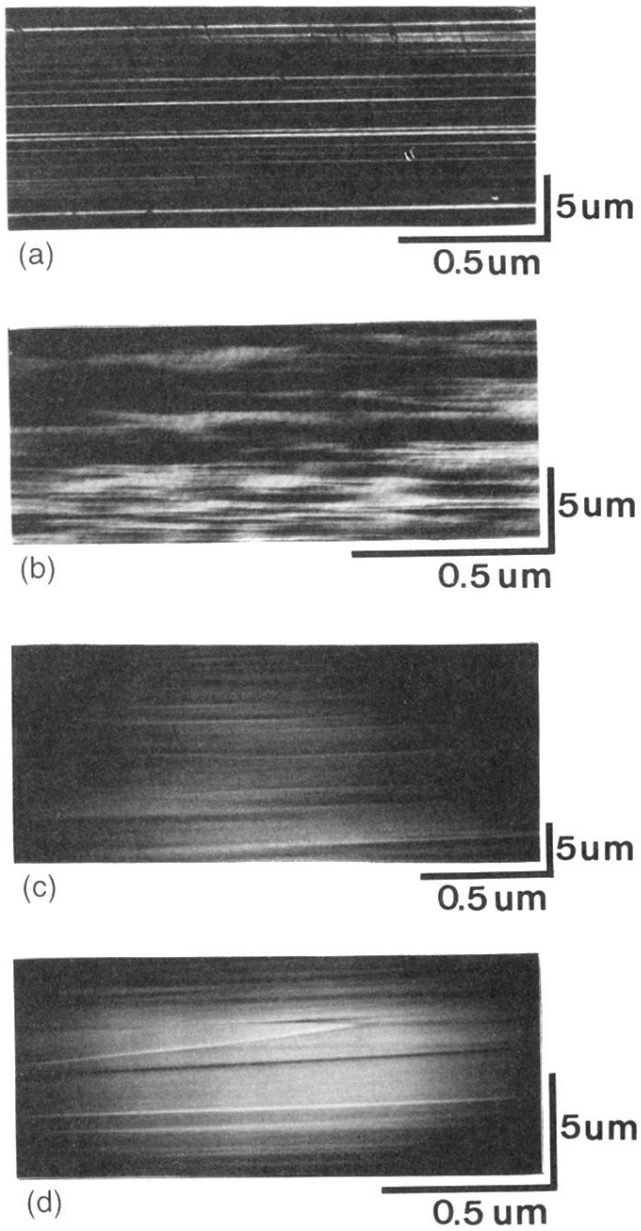

FIG. 3. Reflection electron microscope images on the as-grown diamond (001) surfaces: (a) high-pressure synthetic diamond substrate immersed in H_2 plasma for 15 min; (b) undoped homoepitaxial diamond films formed from $CH_4(5\%)/H_2$; (c) undoped homoepitaxial diamond formed from $CO(5\%)/H_2$; (d) boron-doped homoepitaxial diamond formed from $CO(5\%)/H_2$. The B/C ratio is 2000 ppm.

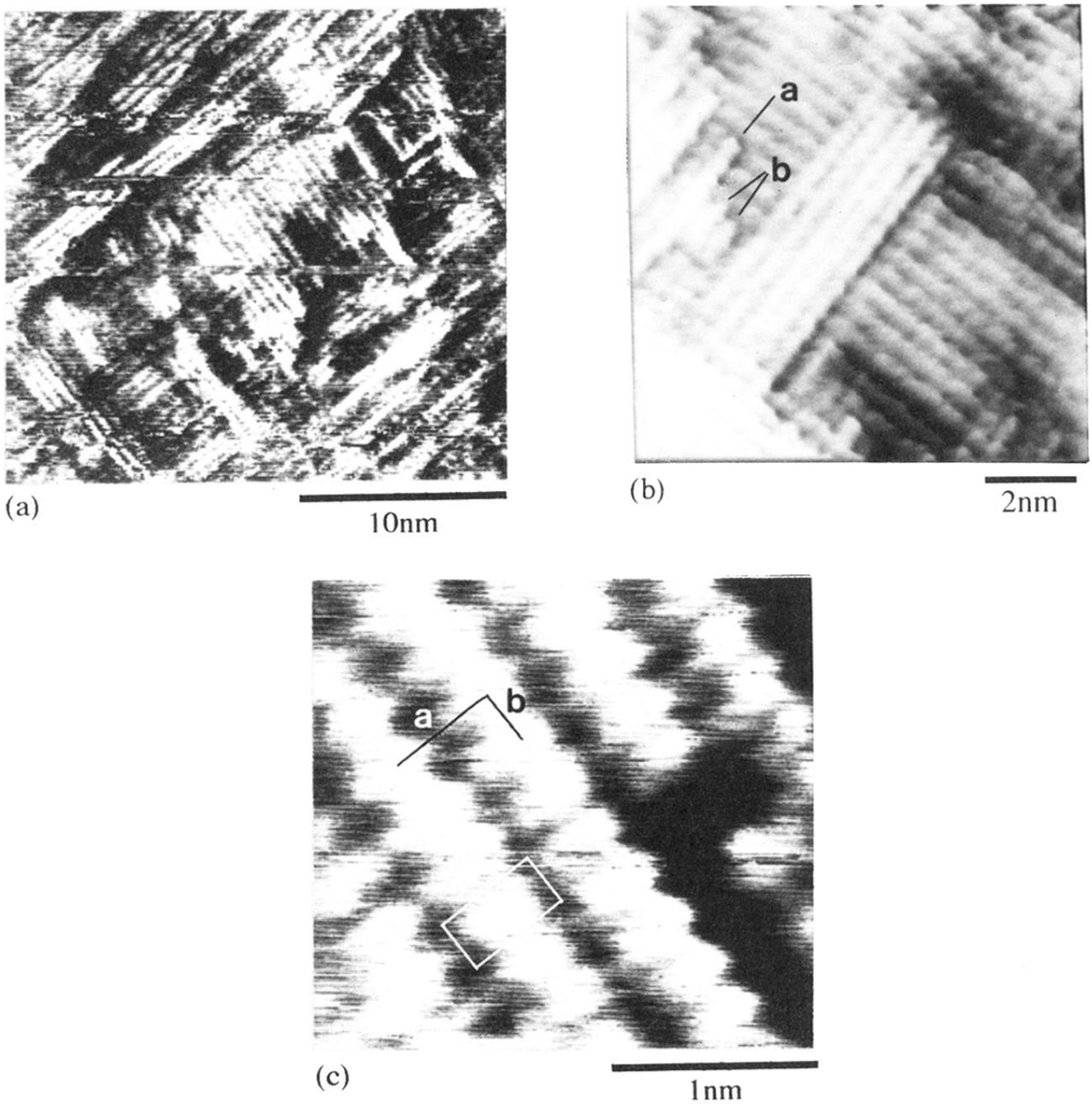

FIG. 4. STM images of undoped and as-grown CVD diamond (001) surfaces formed from CO(5%)/H_2. (a) Current image of 25×25-nm scanned area. The sample bias and tunneling current were −0.05 V and 1 nA. (b) Topographic image of 10×10-nm scanned area. The sample bias and tunneling current were −0.1 V and 3 nA. (c) Current image of 2.5×2.5-nm scanned area. High-magnification image of dimer rows. The length *a* is 0.5 nm and *b* is 0.25 nm. The sample bias and tunnel current were −0.05 V and 1 nA.

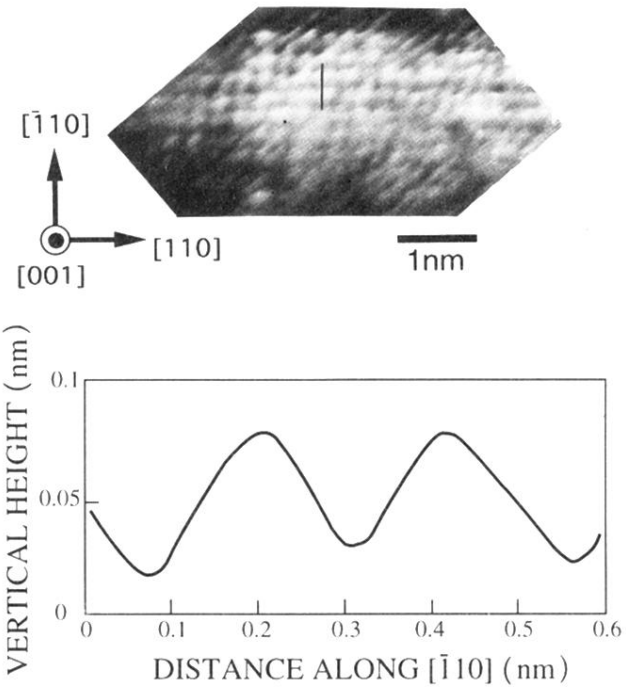

FIG. 6. (a) STM topographic image of undoped and as-grown diamond (001) surfaces formed from CO(5%)/H_2. The substrate bias and tunneling current were 0.5 V and 1 nA. (b) STM corrugation profile of the line marked along the [1$\bar{1}$0] direction.

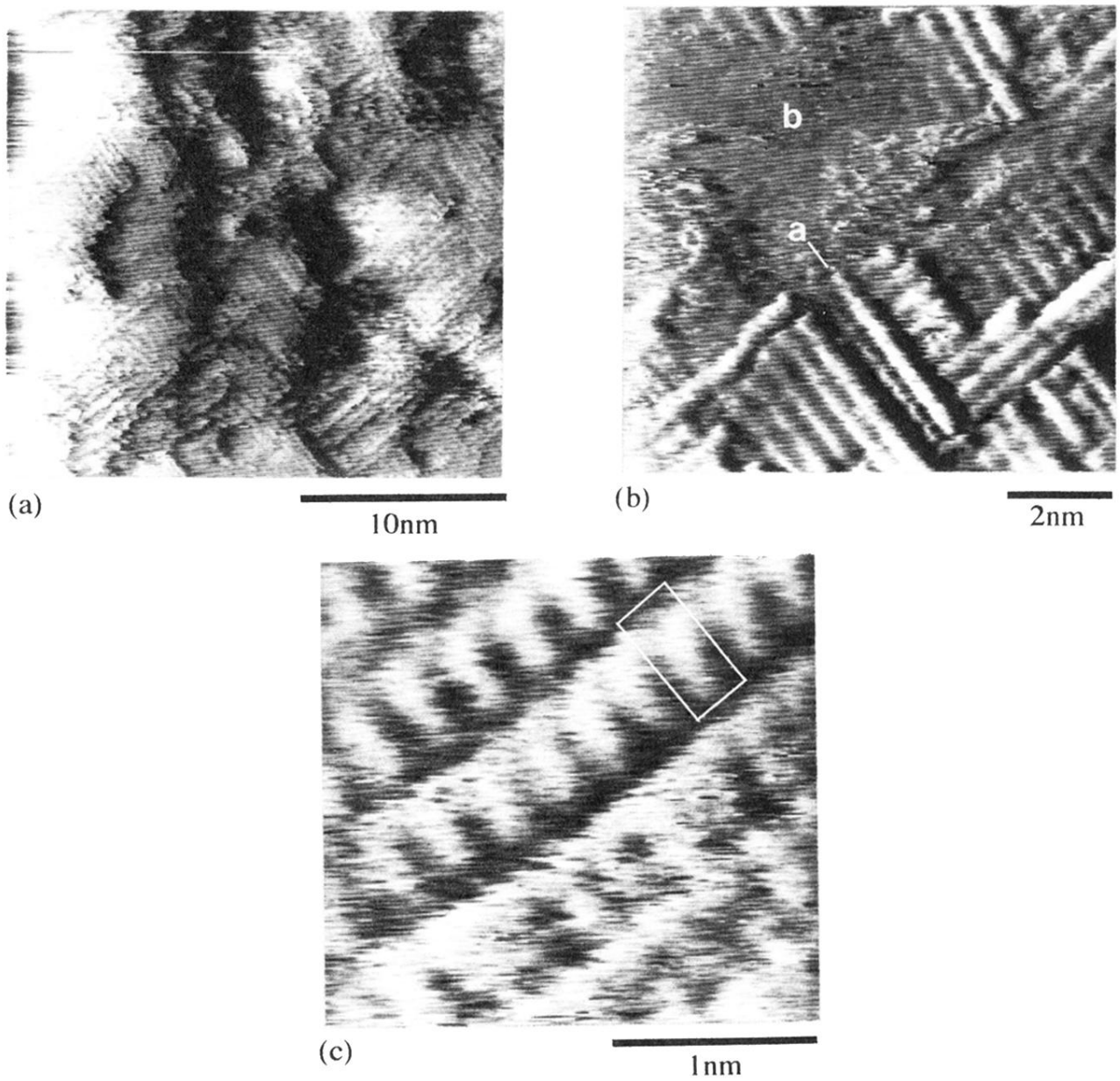

FIG. 8. STM image of boron-doped and as-grown diamond (001) surfaces (B/C 2000 ppm). (a) 25×25-nm scanned area. (b) 10×10-nm scanned area. (c) 2.5×2.5-nm scanned area. All the images were current images obtained at the sample bias of −0.1 V and the tunneling current of 1 nA.

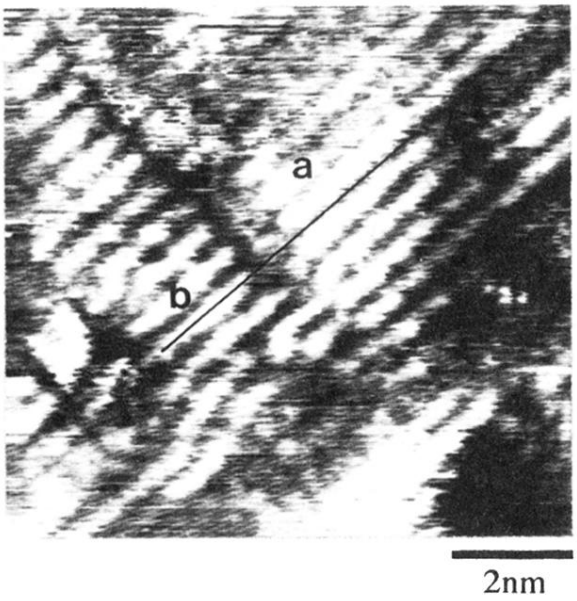

FIG. 9. STM current image of antiphase boundaries on undoped and as-grown diamond film formed from CO(5%)/H_2. The sample bias and tunneling current were -0.05 V and 1 nA.